Macromolecules
ARTICLE

Macromolecules **2010**, *43*, 7845–7851 **7845**
DOI: 10.1021/ma101230v

Polyelectrolyte Brushes: MD Simulation and SCF Theory

Su-zhen He,[†,‡] Holger Merlitz,*[,†,§] Long Chen,[†] Jens-Uwe Sommer,[§] and Chen-Xu Wu*[,†]

[†]*Department of Physics and ITPA, Xiamen University, Xiamen 361005, P.R. China,* [‡]*Department of Electronic Engineering, Putian University, Putian 351100, P.R. China, and* [§]*Leibniz-Institut für Polymerforschung Dresden, 01069 Dresden, Germany*

Received June 1, 2010; Revised Manuscript Received July 14, 2010

ABSTRACT: Off-lattice molecular dynamics simulations are carried out to study fully charged polyelectrolyte brushes with salt, and a comparison with an off-lattice self-consistent field (SCF) theory including finite stretching and volume effects [Biesheuvel et al. *Macromolecules* **2008**, *41*, 6254] is presented. The SCF approach is able to reproduce the brush heights at different grafting densities, salt concentrations, and chain lengths on a semiquantitative level. At high grafting densities, the density profiles obtained with both techniques exhibit a particularly close agreement, while at low densities systematic deviations between their shapes are observed. The approximation of local electroneutrality, which the SCF approach is based on, is studied, and its implications are discussed. In this context, the strengths and limitations of the SCF model are analyzed in detail.

I. Introduction

When chains are densely grafted at one end to a surface, excluded volume interactions are forcing the polymers to stretch away from the grafting surface and form a polymer brush. Polymer brushes have important technological applications which include surface modification, colloidal stabilization, and lubrication.[1] Polyelectrolyte brushes are of particular interest in biological and medical applications because of their hydrophilic nature and interactions with proteins and other biological molecules.

The theoretical understanding of neutral polymer brushes has made significant progress since the seminal works by Alexander and de Gennes.[2,3] Self-consistent-field (SCF) theory[4−7] has been established as a powerful tool for the quantitative understanding of polymer brushes beyond scaling theory. Initial approaches were based on the Gaussian chain approximation. For high grafting densities however, when the chains become strongly stretched, the finite extensibility of chains has to be taken into account.[8−10]

If the grafted polymer is a polyelectrolyte, it contains monomers that dissociate charges in suitable solvents, usually water, and the released counterions generate an osmotic pressure that significantly alters the properties of the brush layer.[11−15] Recently, Biesheuvel et al. have presented an off-lattice SCF model based on the finite stretching solution by Amoskov and Pryamitsyn[7] which displayed rather good agreement with MD simulations of neutral brushes.[16,17] Their equations have been extended to cover charged brushes, but so far the validity of this model has not been verified through computer simulations. The comparison of their SCF approach with MD simulations of charged brushes will be the task of the present paper. In section II, we describe our simulation model, followed by a description of the off-lattice SCF equations and their implementation in section IIIA. We add a detailed discussion of the local electroneutrality approximation in section IIIB because it is of particular relevance for the understanding of the limitations of the SCF approach. Comparisons of the MD and SCF results for systems of different electrostatic interaction strengths are carried out in section IVA, followed by a set of simulations at different grafting densities in section IVB and for different chain lengths and salt concentrations in section IVC. Section V summarizes our findings and evaluates the strengths and limitations of the new SCF approach.

*Corresponding authors. E-mail: merlitz@gmx.de (H.M.); cxwu@xmu.edu.cn (C.-X.W.).

II. Simulation Model

The polyelectrolyte brush was modeled as $M = 64$ freely jointed bead spring chains, anchored at one end to an uncharged planar surface to form a regular 8×8 square grid. The chains were monodisperse and modeled as N spherical beads. The rectangular simulation box with the dimension of $L \times L \times L_z$ had periodic boundaries in both (horizontal) $x-y$ directions, while the (vertical) height was restricted by a wall to confine the salt ions inside the system. The grafting density of the brush is defined as $\sigma = M/L^2$. To achieve electroneutrality of the system, $M \times N \times f$ counterions were added to the simulation box, where f stands for the charge fraction of the brush (i.e., the fraction of charged monomers; we consider only monovalent charges for both monomers and ions throughout this paper). The counterions were modeled as spherical particles of half of the monomer diameter. Additional (monovalent) salt ions were modeled in the same way as the counterions. The LAMMPS molecular dynamics package[18] was used to carry out the simulations.

The total interaction potential was composed of four contributions:

$$U_{\mathrm{tot}} = U_{\mathrm{FENE}} + U_{\mathrm{LJ}} + U_{\mathrm{WALL}} + U_{\mathrm{Coul}} \tag{1}$$

The chains were assumed to be in athermal solvent, modeled by a purely repulsive short-range Lennard-Jones potential

$$U_{\mathrm{LJ}}(r) = 4\varepsilon\left[\left(\frac{d}{r}\right)^{12} - \left(\frac{d}{r}\right)^{6} - \left(\frac{d}{r_{\mathrm{c}}}\right)^{12} + \left(\frac{d}{r_{\mathrm{c}}}\right)^{6}\right] \tag{2}$$

where d stands for the bead diameter and ε defines the strength of the interaction. The parameter r_{c} is the cutoff distance: It is easily verified that without any cutoff ($r_{\mathrm{c}} \to \infty$) this potential has got a minimum at $r_{\mathrm{min}} = 2^{1/6}d$ with the depth $U_{\mathrm{LJ}}(r_{\mathrm{min}}) = -\varepsilon$. In turn,

Published on Web 08/16/2010

once a cutoff $r_c = r_{min}$ is implemented, and the potential shifted up by ε, all attractive contributions to this potential are eliminated and particles inside an athermal solvent are simulated.

Beads along the polymer chains were coupled by a FENE (finitely extensible nonlinear elastic) bond potential[19]

$$U_{FENE} = -0.5KR^2 \ln\left[1-\left(\frac{r}{R}\right)^2\right] + 4\varepsilon\left[\left(\frac{d}{r}\right)^{12} - \left(\frac{d}{r}\right)^{6}\right] + \varepsilon \quad (3)$$

with spring constant $k = 30\varepsilon/d^2$ and maximum bond length $R = 1.5d$. For the chains simulated in this paper, this parameter set delivered an average bond length of $l_{av} = 0.98d$. Naturally, this potential was acting only on chain beads and absent with the counterions or salt ions. The wall was modeled as a 9−3 LJ potential

$$U_{WALL} = \varepsilon\left[\frac{2}{15}\left(\frac{d}{r}\right)^9 - \left(\frac{d}{r}\right)^3\right] \quad (4)$$

with d being the particle size and $\varepsilon = 1$. One wall was located at $z = 0$, the same height as the substrate to which the chains were grafted. An identical wall was placed at $z = L_z$, the upper boundary of the simulation box, to prevent salt ions from escaping the system and diminishing its salt concentration.

The Coulomb interaction was of long-range and had to be addressed with particular care. The simulation package LAMMPS includes the implementation of the particle−particle/particle−mesh (PPPM) algorithm[20−22] that solves the field equation on a lattice through fast Fourier transformation. In this way, the influence of periodic images of charged particles (that show up in both horizontal x- and y-directions) were properly accounted for. Formally, the Coulomb potential is written as

$$U_{Coul}(r) = l_B k_B T \sum_{n_x=-\infty}^{\infty} \sum_{n_y=-\infty}^{\infty} \sum_{i=1}^{N_{tot}-1} \sum_{j=i-1}^{N_{tot}} \frac{q_i q_j}{|\mathbf{r}_{ij} + n_x L\mathbf{e}_x + n_y L\mathbf{e}_y|} \quad (5)$$

where q_i and q_j are the corresponding charges and $l_B = e^2/(4\pi\varepsilon_0\varepsilon k_B T)$ the Bjerrum length, which defines the distance at which both Coulomb energy and thermal energy ($k_B T$) are of the same magnitude. $\mathbf{e}_x$ and $\mathbf{e}_y$ are unit vectors in the $x-y$ direction, and the indices n_x and n_y run over the periodic images of the simulation box. N_{tot} is the total number of charges and L the box size in xy-directions.

The equation of motion was defined as a Langevin equation:

$$m\frac{d^2\mathbf{r}_i}{dt^2} + \varsigma\frac{d\mathbf{r}_i}{dt} = -\frac{\partial U_{tot}}{\partial \mathbf{r}_i} + \mathbf{F}_i \quad (6)$$

where m is the particle mass and ς the friction constant. $\mathbf{F}_i$ is a Gaussian random force that was used to couple the system to the heat bath, with the correlation function

$$\langle \mathbf{F}_i(t)\cdot\mathbf{F}_j(t')\rangle = 6mk_B T\varsigma\delta_{ij}\delta(t-t') \quad (7)$$

The masses of the particles were $m_{mono} = 1$ and $m_{ion} = 0.2$, their diameters were $d_{mono} = 1.0$ and $d_{ion} = 0.5$, the temperature was $k_B T = 0.5\varepsilon$, and the damping constant $\varsigma = 0.5\tau_{LJ}^{-1}$ with $\tau_{LJ} = (md^2/\varepsilon)^{1/2}$ being the Lennard-Jones time.

III. Self-Consistent-Field Model

A. Implementation of the SCF Equations. In this section, the off-lattice SCF model[17] as proposed by Biesheuvel et al. and its numerical implementation are discussed. The SCF equation in the strong-stretching limit is defined as[23,24]

$$V(h) - V(z) = \mu\{\phi(z)\} - \mu\{\phi(h)\} \quad (8)$$

where V denotes the SCF potential as a function of the vertical z coordinate. The mean-field potential μ accounts for the averaged local pair interactions of the monomers and is a function of the (vertical) brush density distribution $\phi(z)$. In what follows, both the z coordinate and brush height h are normalized with the chain contour length $(N-1)\,l_{av}$, so that

$$0 \le z \le h = H[(N-1)l_{av}]^{-1} \le 1 \quad (9)$$

where H denotes the brush height in original units. The potentials are scaled with the thermal energy, $k_B T$. While in most SCF approaches the potential $V(z)$ has to be obtained numerically, Biesheuvel et al. employ an analytical approximation

$$V(z) = 2\frac{z^2}{b}\frac{2-\frac{4}{5}z^2}{1-z^2} \quad (10)$$

Here, b stands for the (nonelectrostatic) Kuhn length, which, contrary to traditional lattice SCF approaches, does not need to equal the monomer size d. Note that this potential contains non-Gaussian contributions to account for the finite extensibility of the chains. For our coarse-grained model, we have determined a Kuhn length of $b \approx 1.3d$ through simulation of a single free chain and application of $\langle R^2\rangle = N^{6/5}b^2$, the mean-square end-to-end distance of an athermal chain.[25]

On the basis of a modified Carnahan−Starling equation of state, which accounts for chain connectivity, and on the assumption of local electroneutrality, the mean-field potential was derived as

$$\mu(\phi) = d^{-1}\left\{\phi\frac{7-7\phi+2\phi^2}{(1-\phi)^3} + \ln(1-\phi)\right\} + \alpha\left\{\sqrt{\left(\frac{\phi}{1-\phi}\right)^2+\gamma^2} - \gamma + \operatorname{asinh}\left\{\gamma^{-1}\frac{\phi}{1-\phi}\right\}\right\} \quad (11)$$

where α denotes the charge fraction number, i.e., the number of charges per unit length along the chain contour, and the parameter γ is defined as

$$\gamma = \frac{2n_\infty v_{bead}}{\alpha d} \quad (12)$$

Here, n_∞ stands for the salt-ion background concentration with a dimension of the inverse volume. Self-consistency of the SCF eq 8 is verified with the help of the mass balance equation

$$\sigma\varpi = \int_0^h \phi(z)\,dz \quad (13)$$

where σ is the grafting density (in numbers per unit area) and ϖ the brush volume per unit chain length. For our bead−spring model with bead diameter d we obtain $\varpi = \pi/(6d^2)$.

To compute the monomer density, the equations presented here are sufficient. A brush height h is proposed, then the equations are numerically integrated, and the mass balance (13) is checked. This procedure is repeated for

different heights until eq 13 is satisfied and hence self-consistency is achieved. As a result, the vertical brush density distribution $\phi(z)$ is obtained. A similar procedure is applied to obtain the vertical end-monomer distribution $g(x)$ of the brush, and we refer to ref 17 for the detailed procedure.

B. Local Electroneutrality Approximation. At the core of the off-lattice SCF theory lies the approximation of local electroneutrality. It is based on the assumption that every horizontal slice of the brush can be regarded neutral; i.e., there exists a charge balance throughout the vertical brush profile. This approximation allows to eliminate the dimensionless electrostatic potential y (which is defined in the Appendix) through

$$2n_\infty(1-\phi)\sinh y = z\alpha d\frac{\phi}{v_{\mathrm{bead}}} \tag{14}$$

and thereby avoids the necessity to solve the Poisson–Boltzmann equation.[17] Naturally, this assumption is limiting the validity of the SCF theory to brushes that are either well inside the osmotic regime, in which practically all counterions are absorbed into the brush, or in the salted regime, when the Debye length is short compared to the brush height such that its screening eliminates every long-range electrostatic interactions.

The same approximation also implies that the SCF equations do not explicitly depend on the Bjerrum length

$$l_{\mathrm{B}} = \frac{e^2}{4\pi\varepsilon\varepsilon_0 k_{\mathrm{B}}T} \tag{15}$$

of the system. The Bjerrum length defines the distance at which both electrostatic and thermal energy are of similar magnitude. If this quantity is expressed in units of the bead size, it serves as a universal measure for the strength of electrostatic interaction in coarse-grained simulation models, in which no physical length scales are available. Previous simulation studies have shown a strong dependence of the brush height on the Bjerrum length.[13,26] As a result of the local electroneutrality approximation, the present SCF approach is unable to reproduce any of these dependencies on the Bjerrum length or, equivalently, on the dielectric constant or temperature of the system. Hence, its validity is restricted to those regimes of the brush which show little dependence on these variables. In the Appendix, additional details concerning the physical basis of the electroneutrality condition are summarized because they are of relevance for the proper interpretation of some of the quantities involved in our simulations.

IV. MD Simulations and Discussion

A. Electrostatic Interaction Strength and Brush Regimes. The systems were initiated as an array of stretched chains grafted in a square lattice pattern onto the substrate ($M = 8 \times 8$). Each chain contained $N = 32$ beads. The ions were modeled as spheres of half of the monomer diameter and distributed all over the simulation box. For relaxation, 4×10^6 simulation steps (corresponding to 6000 LJ times τ_{LJ}) were carried out, followed by several 10^6 simulation steps for data production, during which the conformations were stored after each $3\tau_{\mathrm{LJ}}$.

In a first set of simulations we consider a brush of low grafting density ($\sigma = 0.05d^{-2}$) at different strengths of the electrostatic interaction. In the MD simulation, this was achieved by varying the dielectric constant of the system, leading to a wide range of values for the Bjerrum length (15).

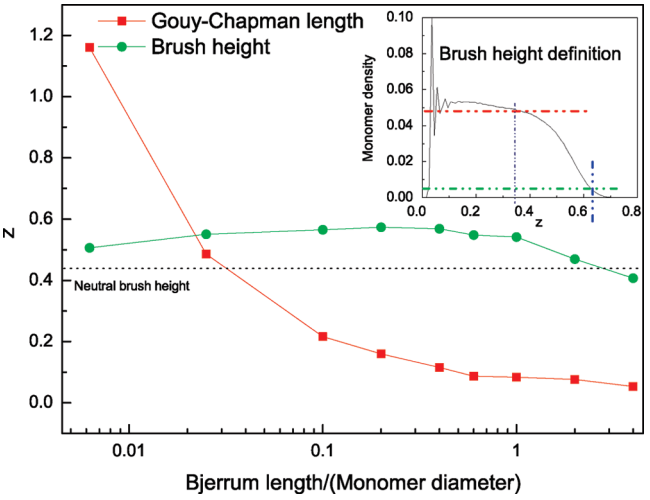

Figure 1. Brush height h and Gouy–Chapman length l_{GC} as a function of the Bjerrum length l_{B}. We distinguish the weak charge regime ($H < l_{\mathrm{GC}}$), the osmotic regime ($H > l_{\mathrm{GC}}$), and the condensation regime ($l_{\mathrm{B}} > 1d$). The inset shows how the brush height was defined (see text for explanations).

The salt concentration was low, $n_\infty = 0.03d^{-3}$, below the salted brush regime that would begin at $n_\infty \approx 0.045d^{-3}$, when the salt concentration reaches the concentration of counterions inside the brush.[12] In this set of simulations, the Debye screening length amounted to roughly $15d$; i.e., it was of the same order as the brush height.

In Figure 1 we display brush height and Gouy–Chapman length as function of the Bjerrum length. The brush height was defined as the vertical coordinate at which the monomer density dropped down to 10% of its average value inside the brush (see inset of Figure 1; in this example, $h \approx 0.625$ was obtained). The average monomer density inside the brush (dashed line in the inset, at density ≈0.05) was determined within the slice between the substrate and the brush center of mass height. The brush was already swollen above its neutral height even at a small Bjerrum length of $l_{\mathrm{B}} = 0.006d$, in agreement with previous simulation results.[13] Although we observed a rather weak swelling ratio less than 50% of the neutral brush height, we note that the stretching factor of chains, as given directly by h (see eq 9), reaches a value close to 0.6.

The Gouy–Chapman length l_{GC} defines the thickness of the counterion layer above the brush surface (i.e., measured above the brush height h). It is common practice to separate the weak charge regime (in which $l_{\mathrm{GC}} > h$) from the osmotic regime ($l_{\mathrm{GC}} < h$), in which most of the counterions are trapped inside the brush. The approximate vertical counterion distribution can be obtained by solving the Poisson–Boltzmann equation,[11] yielding

$$\rho_-(z') = \frac{1}{2\pi l_{\mathrm{B}}(z' - l_{\mathrm{GC}})} \tag{16}$$

where $z' = z - H$ is the vertical distance to the brush surface. Equation 16 can be fitted to the simulated counterion distribution to obtain l_{GC} (squares in Figure 1). The simulation results indicate that for $l_{\mathrm{B}} \geq 0.1d$ the brush had well entered its osmotic regime. Once the product of Bjerrum length and linear charge density (which was fixed to $\alpha = 1$ in our simulations) exceeds unity ($\alpha l_{\mathrm{B}} > 1$), the electrostatic potential close to the monomers becomes comparable in magnitude to the thermal energy of the counterions, and as a result the condensation of counterions sets in.[27] Both the

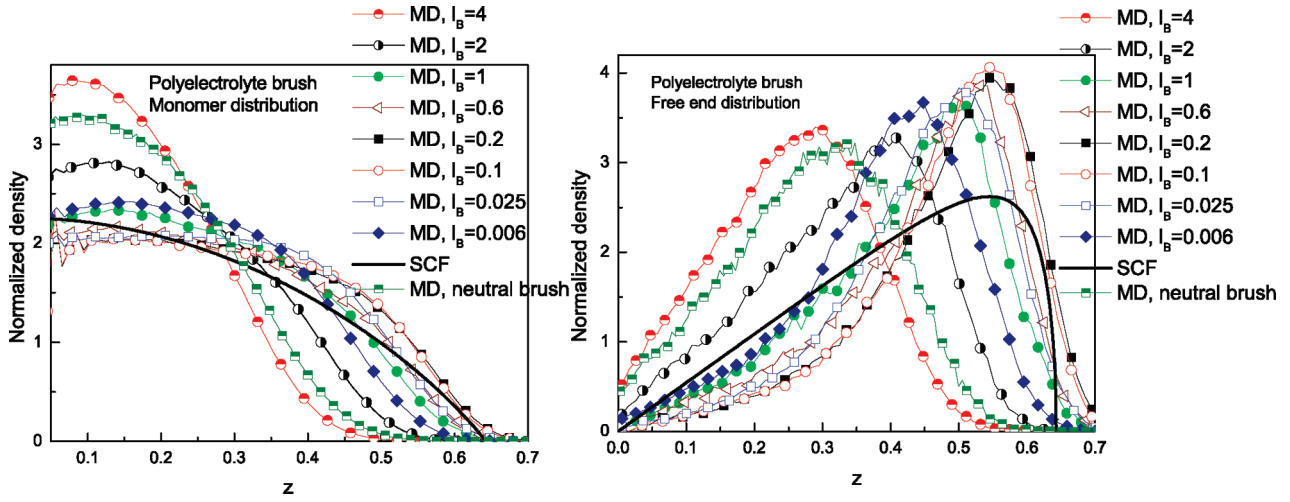

Figure 2. Profiles of monomer density, $\phi(z)$ (left), and end-monomer density, $g(z)$ (right), as a function of the Bjerrum length, l_B, for the same systems as shown in Figure 1. The SCF prediction (solid line) shows a semiquantitative agreement with the brush profiles in the osmotic regime but a poor agreement with the end-monomer densities.

effective charge of the chain and the osmotic pressure of the counterions are diminished in this regime, causing a collapse of the brush. We shall denote this regime as condensation regime. In the extreme case of $l_B > 4d$, the brush had collapsed even below the height of its neutral counterpart. Here, the counterions are firmly adsorbed at the monomers, and residual dipole interactions generate a short-range attraction between monomers which compactifies the brush.

In Figure 2 we display the monomer density profiles (left) and the end-monomer distributions (right) of the various brushes. The SCF results for the charged brush are plotted as continuous curves. As was discussed in section IIIB, due to the local electroneutrality condition, the SCF result does not depend on the Bjerrum length and delivers the same prediction for each of the systems. We would expect the SCF approach to be valid in the osmotic regime and in fact observe a semiquantitative agreement of the brush profiles with the SCF prediction in the range $0.025d \leq l_B \leq 1d$, in which the density profiles display a weak dependence on the electrostatic strength. The simulations consistently deliver profiles that are somewhat more boxlike than the SCF, an observation already made during earlier comparisons with neutral brushes.[17] It should be noted that the location of the crossover between weak and osmotic regime is a function of the grafting density: At higher grafting densities, the osmotic regime is extended toward smaller Bjerrum lengths, so that the validity of the SCF approach is extended as well. The brush collapse in the condensation regime ($l_B > 1d$) is, of course, not reproduced by the SCF theory. There are two reasons for that: First, the mean field is breaking down as soon as the counterions aggregate around the chain contour. Second, the effective charge density, α, is dropping due to counterion adsorption.

The distributions of the end-monomers show a lower degree of agreement with the SCF prediction (right panel of Figure 2). Again, this is consistent with previous simulations of neutral brushes.[17] In fact, SCF theory has never been able to reproduce the simulated end-monomer distributions to a reasonable accuracy, except for the case of high grafting densities. Note that end-monomers are exposed to particularly strong density fluctuations near the brush surface, and it is exactly these fluctuations that are neglected in mean-field theory.

It is instructive to compare the local net charges of the vertical layers of the brush (Figure 3). This quantity serves as

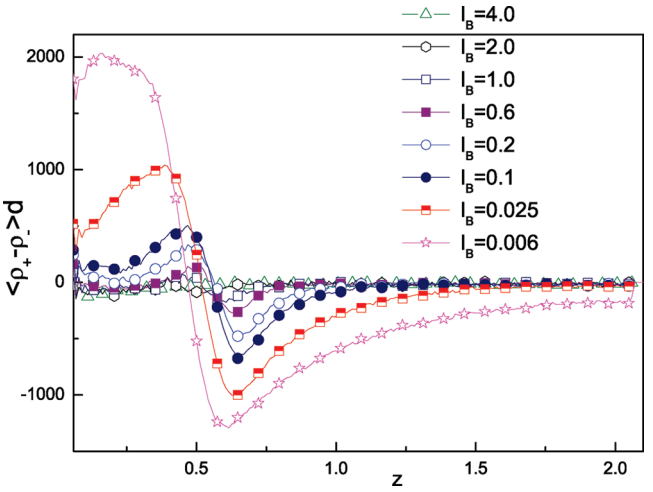

Figure 3. Local net charge $\langle \rho_+ - \rho_- \rangle d$ as a function of the vertical coordinate for different Bjerrum lengths.

a direct evaluation of the validity of the local electroneutrality assumption made in the SCF approach. Not surprisingly, this assumption is satisfied rather well when the Bjerrum length is large (i.e., for strong electrostatics) and less inside the weak charge regime. Throughout the osmotic regime ($0.025d \leq l_B \leq 1d$) there exists a charge separation near the brush surface: The counterions form a charged layer just above the brush, as a result of their osmotic pressure. It is this layer that generates the osmotic pull which contributes to the chain stretch.[12] On the contrary, the local charge neutrality of the osmotic regime is rather well satisfied deep inside the brush. In the case of thick brush layers, when the surface contributes just a small fraction to the brush height, the approximation of local neutrality would turn even more accurate.

B. Brushes at Higher Grafting Densities. In order to study the influence of grafting density, we have simulated chains of length $N = 32$ at a fixed Bjerrum length $l_B = 0.1d$ and with a moderate background salt concentration of $n_\infty = 0.26d^{-3}$ in the density range between $\sigma = 0.1d^{-2}$ and $\sigma = 0.4d^{-2}$, the latter corresponding to an experimental grafting density above 1 chain per squared nanometer. High grafting densities lead to boxlike brush profiles with a high chemical potential gradient at the brush surface.[28,29] The strong

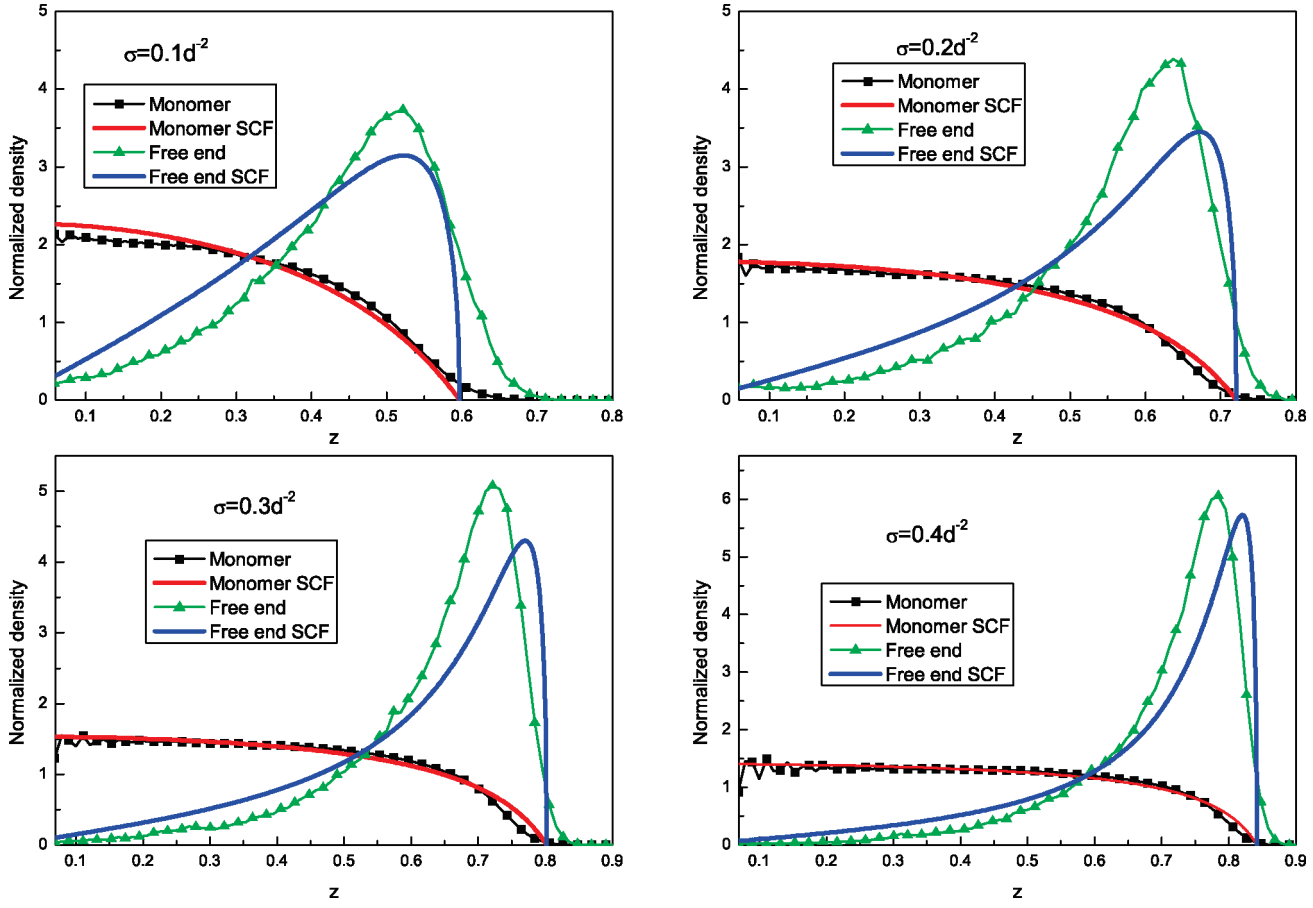

Figure 4. Monomer and end-monomer density profiles at different grafting densities σ. Here, the Bjerrum length was fixed to $l_B = 0.1d$ and the background salt concentration to $n_\infty = 0.26d^{-3}$.

stretching approach is more accurate here, provided that finite extensibility and excluded volume effects (higher virial coefficients) are properly taken into account.

In Figure 4 we display brush profiles and end-monomer profiles at different grafting densities. For these simulations, the brush profiles are generally well reproduced by the SCF theory. In particular, at higher densities, the SCF approach is well able to deliver the boxlike profile which is characteristic for chains with finite extensibility.[28] Even the end-monomer distributions are turning more accurate as the grafting densities increase. This is a result of the reduced fluctuations of the chain ends (which are not accounted for in this SCF approach) under such conditions. The general behavior of the SCF approximation is quite the same as was previously observed with neutral brushes:[17] With increasing grafting density, the results of MD simulations and SCF predictions display an improved degree of agreement.

C. Varying Salt Concentrations and Chain Lengths. The following set of simulations was carried out at moderately low grafting density $\sigma = 0.1d^{-2}$ and moderate Bjerrum length $l_B = 0.1d$. The salt concentrations n_∞ were chosen as $0.05d^{-3}$, $0.09d^{-3}$, $0.13d^{-3}$, and $0.26d^{-3}$. Each of them exceeded the counterion concentration inside the brush, delivering the conditions for the salted brush regime. Different salt concentrations affect the parameter γ as defined in eq 12, and consequently the SCF theory delivers different predictions for the brush profiles. In Figure 5 we compare the results of MD simulations and SCF predictions.

The SCF calculations are well able to reproduce the brush collapse with increasing salt concentration. However, with reduced brush height the shapes of the profiles begin to deviate from the simulation results, quite consistent with our previous observation: While the simulated profiles retain a somewhat boxlike shape, the SCF profiles increasingly turn parabolic once the brush is collapsing. This appears to be a universal feature that is unrelated to the salt concentration, but rather related to the amount of chain stretch: Quite generally, at low brush heights, the SCF profiles are consistently more parabolic than the MD profiles, while in the stronger stretching limit a close agreement is achieved.

For the low salt concentration, brushes of different chain lengths ($N = 32$, $N = 64$, and $N = 96$) have been simulated in order to verify the effects of the brush thickness. As can be seen in Figure 5 (lower right panel), the chain lengths had minor effects on the profiles (which are scaled with the chain contour length, while the SCF theory does not include N as a free parameter, implicitly assuming a long-chain limit). Only the free end distribution of the shortest chains (triangles) displayed an increased level of fluctuations, leading to a somewhat wider peak and an extension that reached slightly further above the brush surface.

Figure 6 verifies that the thickness of the surface ion layer relative to the brush height was diminishing with increasing chain length, so that the electroneutrality condition was satisfied over a wider region of the vertical brush profile. But this fact had little influence on the brush profiles as shown in Figure 5. Consequently, the observed differences between the MD and SCF profiles did not originate in the chain length of $N = 32$, which was selected for computational performance reasons. Considering the fact that the simulations of longer chains would require a substantial investment of computer resources, without significantly

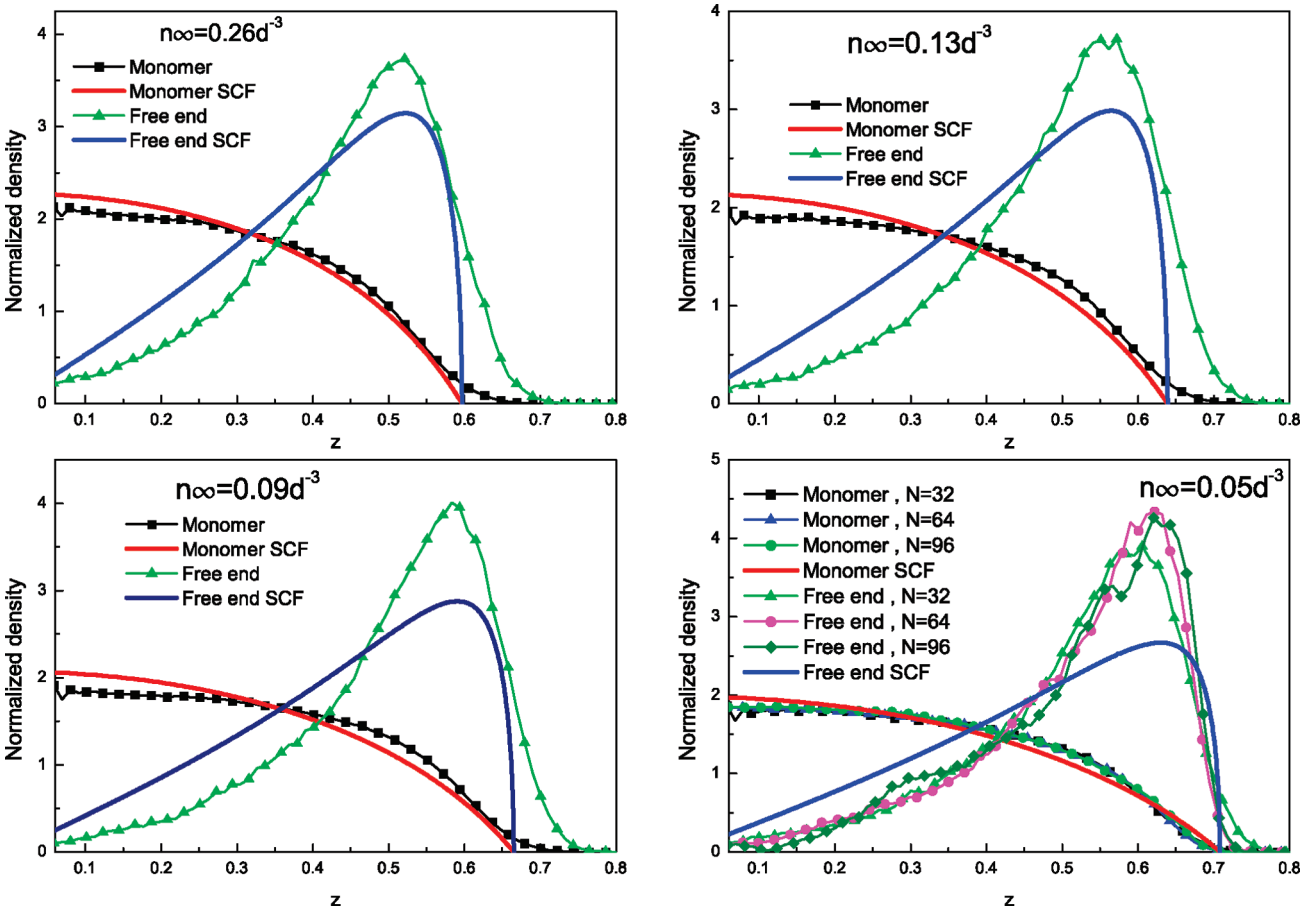

Figure 5. Monomer and end-monomer densities for various salt concentrations n_∞ and γ parameter as defined in eq 12. Simulations with low salt concentration ($n_\infty = 0.05d^{-3}$, lower right panel) were carried out with different chain lengths.

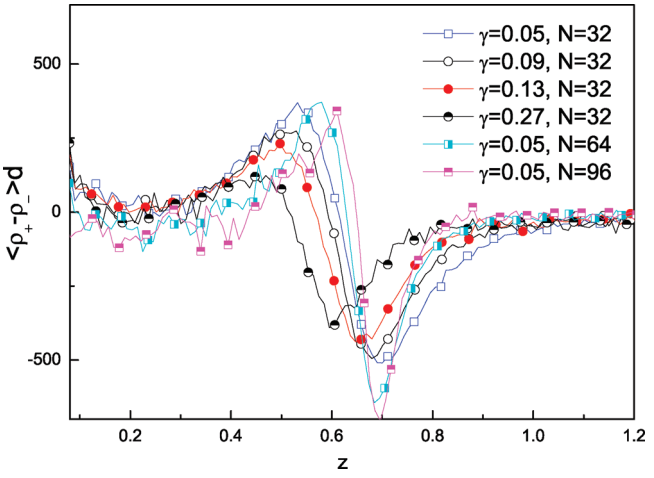

Figure 6. Local net charge $\langle \rho_+ - \rho_- \rangle d$ as a function of the vertical system coordinate for different background salt concentrations and chain lengths.

improving the results over the $N = 32$ case, the choice of shorter chains for the majority of our simulations was justified.

V. Conclusions

In this work we have carried out MD simulations of polyelectrolyte brushes and conducted a comparison with an off-lattice SCF theory that was recently introduced in ref 17. The SCF approach was capable of reproducing the increase of the brush height with the grafting density and its collapse with increasing salt concentration, at semiquantitative accuracy. The validity of the SCF approach is naturally limited to the osmotic brush regime, or the salted brush regime, a consequence of the local electroneutrality approximation (section IIIB). It is therefore unable to reproduce any dependences on the Bjerrum length (i.e., on the dielectric constant or the temperature of the system, Figure 2). This limitation may be tolerable, however, since the validity of the osmotic or salted regime is spanning a broad parameter range over which the brush profiles display just a minor dependence on the Bjerrum length.

A rather good agreement of the density profiles was found at higher grafting densities (Figure 4), while at lower densities, the MD profiles were consistently deviating from the SCF predictions, the former being rather boxlike and the latter rather parabolic. This appears to be an inherent feature of this SCF approach and had previously been observed during a comparison with neutral brushes.[17] Additional studies are required to pinpoint the origin of this deficiency. The strong-stretching limit, eq 8, is reducing the chain conformations to their classical paths, neglecting random fluctuations of their contours. This would explain its relatively high accuracy at high chain stretch when exactly these fluctuations are diminished. It remains to be verified whether or not a relaxation of the strong-stretching limit would extend the good performance of this approach toward the lower chain stretch regime.

The distributions of end-monomers were generally displaying poor agreement between the MD and SCF approach, except for the case of very high grafting densities. It should be pointed out that SCF theory has never been very successful in reproducing end-monomer distributions. This is, at least in parts, the

consequence of density fluctuations, which are particularly high near the brush surface where the chain ends spend most of their time. Quite naturally, no mean-field approximation should be expected to perform well in this region of the brush. However, a relaxation of the strong-stretching limit may again have the potential to improve the agreement with the simulations, but this would naturally affect the simplicity of the SCF procedure.

In summary, the SCF approach is able to deliver quantitative predictions for the brush profiles in the osmotic or salted regime in the case of strong chain stretch, and semiquantitative predictions in the case of low chain stretch. On the basis of a semianalytic off-lattice formalism, it incorporates features like finite chain extensibility, packing constraints, variable Kuhn lengths, and monomers of arbitrary size without the need of any parameter fitting. As was shown elsewhere,[16] the approach is flexible enough to incorporate particles of different charges or sizes. These are certainly strong points in support of this formalism, while previous approaches were either restricted to low-density brushes (due to the Gaussian approximation of the chain stretch) or required a parameter fit in order to achieve quantitative agreement with simulations.

Acknowledgment. We thank P. M. Biesheuvel (Wageningen University, The Netherlands) for fruitful discussions. This work was supported by the National Science Foundation of China under Grant Nos. 50873083 and 10974162.

Appendix. Local Electroneutrality Condition

The following discussion is based on the work of Zhulina et al.[30] It serves as a clarification of the meaning of the background salt concentration n_∞ and the assumptions on which the local charge electroneutrality approximation is based. We have to distinguish between two electroneutral subsystems: the brush and the bulk solution. c_p is the molar concentration of monomers, and α is the charge fraction of a quenched polyelectrolyte brush. We define c^- and c^+ as the total concentrations of mobile ions inside the brush, i.e., $c^- = \sum_i c_i^-$ and $c^+ = \sum_i c_i^+$, summing up all types of salt ions and counterions. Global electroneutrality in the polyacid brush then implies

$$\alpha c_p + c^- = c^+ \tag{17}$$

For the bulk solution, the same condition demands

$$C^+ = C^- \tag{18}$$

where $C^- = \sum_i C_i^-$, $C^+ = \sum_i C_i^+$, and capital letters stand for mobile ion concentrations in the bulk, i.e., in the absence of the brush. These separate conditions for electroneutrality account for the fact that mobile ion distributions are modified in the presence of the brush, when compared to their distributions in the bulk. This redistribution is caused by the excess electrostatic potential Ψ, where *excess* refers to an effective potential generated by the brush and its counterions. If the ions are regarded as point charges, and neglecting effects of excluded volume due to the brush chains, the equilibrium distributions follow the Boltzmann law

$$c_i^+ = C_i^+ \exp(-y) \tag{19}$$

and

$$c_i^- = C_i^- \exp(y) \tag{20}$$

where $y = e\Psi/(k_B T)$ is the dimensionless electrostatic potential. The two previous relations satisfy the Donnan rule

$$c_i^+ / C_i^+ = C_i^- / c_i^- > 1 \tag{21}$$

and the combination with the electroneutrality condition eq 17 then yields the total concentration of mobile ions inside the brush:

$$(c^+ + c^-)^2 = \alpha^2 {c_p}^2 + 4C^+ C^- \tag{22}$$

After inserting $c^- = C^- \exp(y)$ and $c^+ = C^+ \exp(-y)$, we finally arrive at the local electroneutrality condition:

$$2C^+ \sinh(y) = \alpha c_p \tag{23}$$

This has to be compared with eq 14 to deliver n_∞ as the salt concentration in bulk solution.

References and Notes

(1) Netz, R. R.; Schick, M. *Macromolecules* **1998**, *31*, 5105.
(2) deGennes, P. G. *Macromolecules* **1980**, *13*, 1069.
(3) Alexander, S. *J. Phys.* (*Paris*) **1977**, *38*, 977.
(4) Semenov, A. N. *Sov. Phys. JETP* **1985**, *61*, 733.
(5) Milner, S. T.; Witten, T. A.; Cates, M. *Macromolecules* **1988**, *21*, 2610.
(6) Wijmans, C. M.; Scheutjens, J. M. H. M.; Zhulina, E. B. *Macromolecules* **1992**, *25*, 2657.
(7) Amoskov, V. M.; Pryamitsyn, V. A. *J. Chem. Soc., Faraday Trans.* **1994**, *90*, 889.
(8) Shim, D. F. K.; Cates, M. E. *J. Phys.* (*Paris*) **1989**, *50*, 3535.
(9) Matsen, M. W. *J. Chem. Phys.* **2004**, *121*, 1938.
(10) Lai, P. Y.; Halperin, A. *Macromolecules* **1991**, *24*, 4981.
(11) Pincus, P. *Macromolecules* **1991**, *24*, 2912.
(12) Borisov, O. V.; Zhulina, E. B.; Birshtein, T. M. *Macromolecules* **1994**, *27*, 4795.
(13) Rühe, J.; Ballauff, M.; Biesalski, M. *Adv. Colloid Interface Sci.* **2004**, *165*, 79.
(14) de Vos, W. M.; Biesheuvel, P. M.; de Keizer, A.; Kleijn, J. M.; Stuart, M. A. C. *Langmuir* **2008**, *24*, 6575.
(15) Biesheuvel, P. M. *J. Colloid Interface Sci.* **2004**, *275* (1), 97.
(16) de Vos, W. M.; Biesheuvel, P. M.; de Keizer, A.; Kleijn, J. M.; Stuart, M. A. C. *Langmuir* **2009**, *25*, 9252.
(17) Biesheuvel, P. M.; de Vos, W. M.; Amoskov, V. M. *Macromolecules* **2008**, *41*, 6254.
(18) Plimpton, S. J. *J. Comput. Phys* **1995**, *117*, 1.
(19) Kremer, K. *J. Chem. Phys.* **1990**, *92*, 5057.
(20) Hockney, R.; Eastwood, J. *Computer Simulation Using Particles*; McGraw-Hill Inc.: New York, 1981.
(21) Frenkel, D.; Smit, B. *Understanding Molecular Simulations*; Academic Press: New York, 2001.
(22) Pollock, E. L.; Glosli, J. *Comput. Phys. Commun.* **1996**, *95*, 93.
(23) Milner, S. T.; Witten, T. A.; Cates, M. E. *Macromolecules* **1988**, *21*, 2610.
(24) Zhulina, E. B.; Pryamitsyn, V. A.; Borisov, O. V. *Polym. Sci. USSR* **1989**, *31*, 205.
(25) Csajka, F. S.; Netz, R. R.; Seidel, C.; Joanny, J. F. *Eur. Phys. J. E* **2001**, *4*, 505.
(26) Arun, K. N.; Christian, S. *Macromolecules* **2005**, *38*, 9341.
(27) Dobrynin, A. V.; Colby, R. H.; Rubinstein, M. *Macromolecules* **1995**, *28*, 1859.
(28) He, G.-L.; Merlitz, H.; Sommer, J.-U.; Wu, C.-X. *Macromolecules* **2007**, *40*, 6721.
(29) Merlitz, H.; He, G.-L.; Wu, C.-X.; Sommer, J.-U. *Macromolecules* **2008**, *41*, 5070.
(30) Zhulina, E. B.; Birshtein, T. M.; Borisov, O. V. *Macromolecules* **1995**, *28*, 1491.